GA-A14897

EVALUATION OF SPRAYED CHROMIUM CARBIDE COATINGS FOR GAS-COOLED REACTOR APPLICATIONS

by
G. Y. LAI

This is a preprint of a paper to be presented at the International Conference on Metallurgical Coatings, April 3-7, 1978, San Francisco, California, and to be printed in the Proceedings.

Work supported in part by
Department of Energy
Contract EY-76-C-03-0167, Project Agreement No. 65

GENERAL ATOMIC PROJECT 3273
FEBRUARY 1978

GENERAL ATOMIC COMPANY

ABSTRACT

Sprayed chromium carbide-nichrome coatings are candidates for protection of faying and sliding surfaces of critical components of gas-cooled reactors from friction and wear damage. These coatings must provide protection throughout the reactor lifetime under high temperature exposure conditions. Extensive evaluation work to characterize these coatings is underway. The work includes studies of friction and wear behavior in helium; stability of the coatings in a low oxygen potential helium environment; impure helium corrosion of coated specimens; and the effect of the coatings on mechanical properties of the substrate alloy. Much of the work reported is on the evaluation of plasma-sprayed coatings. However, a brief discussion of the behavior of coatings applied by the detonation-gun process and high-energy plasma-gun processes is also included.

CONTENTS

TABLES

TABLES (Continued)

FIGURES

1. INTRODUCTION

In a high temperature gas-cooled reactor (HTGR) high-pressure helium is used as the primary coolant for removing the fission heat from the reactor core. In the case of steam-cycle HTGR systems, this fission heat is transferred via the steam generators to the water/steam secondary coolant which drives turbogenerators to produce electricity. This primary coolant helium generally contains low levels of gaseous impurities, such as H_2, CO, CH_4, H_2O, etc. These impurities may come from various sources, such as outgassing of the core, reactions of the core graphite with ingress water, proton diffusion, etc. (1)*. This environment, which generally contains a very low oxygen partial pressure, may inhibit the formation of protective oxide films on the metal surface when exposed to elevated temperatures. The relative movement of unprotected mating surfaces of components could lead to a potential component failure due to high friction, galling, self-welding and fretting. It is thus necessary to apply protective coatings to the metal surfaces wherever needed to preclude or minimize this type of damage.

Sprayed chromium carbide based coatings are considered for use in many structural components, such as the thermal barrier and steam generators. The coatings must function adequately for the reactor's 40-year design life.

---

*Number in brackets denotes references at the end of paper.

They must "remain" on the substrate, maintain adequate friction and wear-resistant properties, and be compatible with the substrate material. This paper summarizes the results of an on-going evaluation program on sprayed chromium carbide based coatings.

2. MATERIALS AND TEST METHODS

2.1. COATING MATERIALS

Coatings under evaluation are either Cr_3C_2- or $Cr_{23}C_6$-based. Most of the coatings evaluated were applied by plasma processes. However, some tests were performed on Detonation-gun* (D-gun) applied coatings and coatings applied by high-energy plasma processes, such as Plasmadyne's Mach 2 system and Pratt and Whitney's Gator-Gard process. The nominal coating thickness was 0.004 in. (0.01 cm). The powder used for spraying was a homogeneous mechanical blend of chromium carbide (either Cr_3C_2 or $Cr_{23}C_6$) and nichrome (NiCr) powders. The nichrome is a NiCr alloy consisting of 80 wt % Ni and 20 wt % Cr. The powders used for plasma spraying consisted of 75 wt % chromium carbide and 25 wt % nichrome, while those used for D-gun spraying consisted of 80 wt % chromium carbide and 20 wt % nichrome. The powders generally exhibited the following particle size distribution: (a) Carbide powder: -270 mesh/99.5% min, -325 mesh/98% min, -20 μm/75% min, and -5 μm/20% max; (b) NiCr powder: -270 mesh/100% min, +325 mesh/1% max, -20 μm/60% min, and -5 μm/15% max.

2.2. SUBSTRATE MATERIALS

The substrate alloys used in this investigation are tabulated in Table 1.

---

*Proprietary process of Linde Division (Union Carbide).

2.3. TEST METHODS

2.3.1. Friction and Wear Tests

Friction and wear tests were conducted on the specimens with a button-on-plate arrangement and flat-on-flat interface configurations with reciprocative motions. The test apparatus was described in detail in a previous report (2). In this investigation a triple reduction gear, which is capable of producing an average sliding velocity of 1 in. (2.54 cm)/ hr, was used. The test chamber is connected to a once-through helium system which generates a simulated HTGR helium environment for friction and wear tests. The test gas was fed into the test chamber and then exhausted to the atmosphere. The gas flow was kept at about 500 cc/min throughout the test. The test environment consisted of purified helium at 1.3 atm pressure with the following nominal gaseous impurities: 200 μatm H_2, 20 μatm CH_4, 10 μatm CO, and approximately 1 μatm H_2O. This environment was produced by purifying the reactor grade helium by passing it through an activated charcoal liquid nitrogen cold trap and then injecting the desired quantities of H_2, CH_4 and CO to make up the test gas. No water was injected into the system. Nevertheless, measurements of partial pressure of oxygen (P_{O_2}) in the test environment at temperatures of interest by an oxygen probe indicated that the measured P_{O_2} was equivalent to 1 μatm H_2O in equilibrium with 200 μatm H_2. A detailed description of this once-through helium system is given elsewhere (3). Measurements of gaseous impurities by a gas chromatograph were made daily except weekends and holidays. Variations of H_2, CO, and CH_4 were within ±20%. These variations did not result in any significant changes in H_2O levels.

The surface roughness of test specimens was measured by a profilometer. Specimens were cleaned in acetone and weighed in a precision balance prior to installation in the test rig. Following testing the specimens were subjected to detailed examination which included some, or all, of the following: (1) visual examination of the wear track, (2) weight measurements, (3) profilometer measurements of the wear track, (4) scanning electron microscopy examination, (5) optical metallographic examination, and (6) examination of wear debris.

2.3.2. Helium Compatibility Tests

High-purity alumina retorts connected to the once-through helium system were used for elevated-temperature exposure tests. The test environment consisted of purified helium at 1.3 atm pressure with the following nominal gaseous impurities: 200 μatm H_2, 20 μatm CH_4, 10 μatm CO, and approximately 1 μatm H_2O. The test gas (supplied by the same helium system as the friction and wear tests) was fed into each retort and then exhausted to atmosphere. The gas flow was kept at about 100 cc/min throughout the test. The temperature in the retort was continuously measured by a multipoint recorder and was maintained at the nominal ±5°C.

Specimens were cleaned with acetone before being placed in the retort. The retort was then evacuated and purged several times with the test gas until no air contamination was detected by a gas chromatograph. The retort was then heated to the test temperature. After a specified exposure time, the retort was furnace-cooled to room temperature with the test gas flowing.

The specimens were then examined visually for spallation and replaced in the retort for more exposure if no spallation was observed. The time intervals for examination of coated specimens were 50*, 100*, 500*, 500, and 1000 hr at 1800° (982°C), 1700° (927°C), 1600° (871°C), 1500° (816°C), and 1400°F (760°C), respectively.

2.3.3. Low Cycle Fatigue and Creep Rupture Tests

Both low cycle fatigue and creep rupture tests were conducted in air. The low cycle fatigue testing was performed in an MTS system using constant axial strain control. An axial strain rate of 4×10^{-3}/sec was used. The test method is similar to that developed by Slot, et al., featuring the use of hour-glass shaped specimens with diametral strain measurements (4). The coating was not taken into account in the diametral strain measurements based on the assumption that it was too thin to significantly affect the strain measurements. The creep rupture testing was conducted in accordance with ASTM E139-70 at a constant load in a level arm creep machine. The stress applied was based on the cross-sectional area of the specimen prior to the application of the coating. The strains were measured using an optical extensometer system. A detailed description of this type of extensometer is given elsewhere (5).

---

*First three examinations were made after 25, 50 and 100 hr exposure at 1800° (982°C) 1700° (927°C) and 1600°F (871°C), respectively.

3. RESULTS AND DISCUSSION

The results discussed in this paper are a summary of the data generated to date from an on-going evaluation program. The whole program covers many aspects of investigation. This paper, however, reports only the results of friction and wear, helium compatibility, and the effects of the plasma-sprayed coating on low cycle fatigue and creep rutpure properties of the substrate alloy.

3.1. FRICTION AND WEAR BEHAVIOR

Previous friction and wear studies (2) on austenitic alloys, such as Alloy 800 and Hastelloy X, rubbing against themselves at 1472°F (800°C) in helium* indicated adhesive wear with a friction coefficient ranging from approximately 1.7 to 2.5 during sliding up to 60 meters. Evidence of strong localized self-welding between the mating surfaces was observed when specimens were examined after testing. However, a considerably lower friction coefficient (0.3 to 0.4) was observed when the test specimens were plasma sprayed with a Cr_3C_2-NiCr coating and tested under similar conditions (2). In the above studies, an average sliding velocity of approximately 1000 in (2540 cm)/hr** was used for the tests.

---

*Reactor grade helium.

**35 cycles/min with 0.5 in. (12.7 mm)/cycle.

In certain HTGR components (such as the thermal barrier), relative sliding between two mating surfaces results from thermal expansion and contraction of materials during thermal transients. Since temperature changes occur slowly in the HTGR, this means that sliding velocities are, in fact, much slower than those used in the earlier tests. For example the average sliding velocity expected in the thermal barrier of an HTGR ranges from 1 in (2.54 cm)/hr to 0.1 in. (0.254 cm)/hr. Friction and wear tests at these low velocities are currently underway to address the possible effects of the sliding velocity. The test results so far have revealed two significant observations: (1) a considerably higher friction coefficient was observed when tested at 1 in. (2.54 cm)/hr as compared to 1000 in. (2540 cm)/hr, as illustrated in Fig. 1, and (2) severe chattering (stick-slip) such as the one shown in Fig. 2 was observed in the low velocity tests. The chattering which generally occurred during initial sliding disappeared after some distance of sliding. For example, the chattering occurred during the initial 75 in. (190 cm) and 20 in. (50.8 cm) of sliding for D-gun applied $Cr_{23}C_6$-NiCr and Cr_3C_2-NiCr coatings, respectively.

The above observations are, of course, very preliminary. The tribology of these sprayed coatings at low sliding velocities is complex in nature. An extensive test program is currently underway to characterize the tribological behavior as a function of various parameters, such as coating properties, load, temperature, sliding velocities, helium chemistry, etc. The results of these further investigations will be reported at a later date.

3.2. HTGR HELIUM COMPATIBILITY

3.2.1. Thermal Stability of Coatings

The phase stablility in both Cr_3C_2- and $Cr_{23}C_6$-based coatings during exposure to a simulated HTGR helium is under evaluation. The results reported here include only Linde's plasma-sprayed coatings exposed at 1600°F (871°C). Table 2 summarizes the phases present in the plasma-sprayed Cr_3C_2-NiCr and $Cr_{23}C_6$-NiCr coatings. It is evident from the table that the amount of Cr_7C_3 phase formed in the Cr_3C_2-NiCr coating after exposure for 520 hrs was significantly higher than the coating exposed for 1 hr. This suggests that the structural change of carbides from Cr_3C_2 to Cr_7C_3 had taken place during the exposure. It is not clear, however, about the change of the predominant carbide phase from $Cr_{0.62}C_{0.35}N_{0.03}$ in the as-coated condition to Cr_3C_2 in the 1-hr exposed sample. In the as-coated condition the Cr_3C_2 diffraction lines were relatively sharp, while all the lines assigned to $Cr_{0.62}C_{0.35}N_{0.03}$ were broad and diffuse suggesting that this carbide phase (a_o = 6.962 Å, b_o = 9.192 Å, and c_o = 2.838 Å) may be a "distorted" structure of Cr_3C_2 (a_o = 5.528 Å, b_o = 11.475 Å, and c_o = 2.829 Å) resulting from non-stoichiometry of carbides and/or the rapid quench of carbide particles from the molten state during spraying. The short-time exposure at 1600°F (871°C) then could have restored the structure to that of Cr_3C_2. Taylor (6) did not detect $Cr_{0.62}C_{0.35}N_{0.03}$ phase in the as-deposited condition of Linde's plasma-sprayed Cr_3C_2-NiCr coating, but observed both Cr_3C_2 (major phase) and Cr_7C_3 (minor phase) along with NiCr phase.

For the $Cr_{23}C_6$-NiCr coating, the predominant carbide phase remains $Cr_{23}C_6$ even after exposure up to 2700 hrs. A small amount of Cr_7C_3 was detected in the short time exposed sample, and is believed to have been transformed to $Cr_{23}C_6$ (a more stable form of chromium carbide) upon further exposure at 1600°F (871°C). X-ray analysis of Linde's $Cr_{23}C_6$ powders showed the presence of a small amount of Cr_7C_3. The Cr_7C_3 phase was not detected in the as-deposited coating. This is probably due to the fact that the observed diffraction lines were few and diffuse (weak patterns) which make it difficult to completely identify the phases present. It is thus believed that no changes in carbide structures occurred during plasma spraying. The minor Cr_2O_3 oxide phase observed in the short time exposed sample could be formed during plasma spraying and/or during exposure in the helium environment. The formation of $FeCr_2O_4$-type spinels in the 2700-hr exposed sample is believed to be the result of long-term exposure to the helium environment.

There exist three forms of chromium carbides, namely Cr_3C_2, Cr_7C_3, and $Cr_{23}C_6$. Their relative thermodynamic stabilities are reflected by their standard free energies of formation. Of the three forms of chromium carbides, $Cr_{23}C_6$ is the most stable compound, while Cr_3C_2 is the least. Due to the fact that $Cr_{23}C_6$ is the most chromium rich carbide, $Cr_{23}C_6$ would be expected to be the equilibrium carbide phase in a low-carbon and high-chromium alloy (e.g., NiCr binder or Alloy 800 substrate).

3.2.2. Impure Helium Corrosion

The coated specimens were exposed to a simulated HTGR helium environment in the temperature range from 1200° to 1800°F (649° to 982°C) for various times. Several coated specimens which had not spalled as a result of exposure were subjected to metallurgical examination. Figure 3 shows typical structures of Linde's plasma $Cr_{23}C_6$-NiCr coated Alloy 800H specimens after exposure at 1200°, 1400° and 1600°F (649°, 760° and 871°C) for approximately 1000 hr. In addition to internal oxidation in the substrate, significant oxidation was observed to occur on the substrate surface at the coating-substrate interface after exposure at 1600°F (871°C). Only slight substrate surface and internal oxidation was observed after exposure at 1400°F (760°C) for 1000 hr. The structure of the coating-substrate interface after exposure at 1200°F (649°C) for 1000 hr was essentially the same as that of the as-coated condition.

Continued exposure at 1600°F (871°C) resulted in spallation of the coating from the substrate. Figure 4 shows the appearance of Alloy 800H specimens coated with a plasma-sprayed $Cr_{23}C_6$-NiCr coating (Linde's coatings) after exposure at 1600°F (871°C) for three different times. The coating was intact after 1578 hr. However, the coating at the coated edge was observed to spall off from the substrate after 1914 hr. Gross spallation of the coating occurred after 2610 hr.

Metallurgical evaluation of the Alloy 800 (or Alloy 800H) substrate surface where the coating (either Cr_3C_2- or $Cr_{23}C_6$-based coating) had spalled off showed the presence of oxides. Electron microprobe analysis indicated that the oxides were rich in Cr, Mn, Si, Ti and Al, and depleted in Ni and Fe. The oxygen potential measured in the test environment was oxidizing to Cr, Mn, Si, Ti and Al, but reducing to Ni and Fe (assuming unit activity for the above elements). Similar oxidation behavior was observed by Mazandarany (3) in his studies of gas - metal reactions in a simulated HTGR helium environment.

The plasma-sprayed chromium carbide coatings are considered to be relatively porous with respect to gaseous species. The gaseous species can permeate through the coating and react with the substrate. The grit blasting process, which roughens the substrate surface prior to plasma spraying, may increase the surface energy of the substrate making it more reactive. The Cr activity in the "binary" NiCr binder is much lower than that in the "ternary" Fe-Ni-Cr substrate (e.g., Alloy 800) (7). These, coupled with the presence of Si, Mn, Ti and Al (very active elements) in the substrate, tend to produce stable oxides much more readily in the substrate - hence preferential oxidation at the interface.

3.2.3. Spallation of Coatings

From the discussion in the last section, it is evident that the exposure of plasma-sprayed Cr_3C_2-NiCr or $Cr_{23}C_6$-NiCr coated specimens to the impure helium at elevated temperatures (e.g., 871°C) results in the formation of corrosion products (oxide phases) at the coating-substrate interface. The interfacial oxides are a result of oxidation of the substrate

surface. The oxidation of substrate surface continues with increasing exposure time until most of the interfacial area is covered by oxides. Gross spallation of the coating then occurs. Apparently the interfacial oxides weaken the coating-substrate bonding. In addition, the thermal expansion coefficient mismatch between the coating and the substrate alloy may produce some residual stresses in the coating which could further contribute to spallation.

The instability of the carbide phase in the coating can further promote spallation. It is found that Linde's plasma-sprayed Cr_3C_2-NiCr coating spalled from the substrate Alloy 800 (or Alloy 800H) at a considerably shorter exposure time as compared to Linde's plasma-sprayed $Cr_{23}C_6$-NiCr coating applied to the same substrate, even though both types of coatings exhibited similar microstructure and bond strength. The structural change of carbides from Cr_3C_2 to Cr_7C_3 in the plasma-sprayed Cr_3C_2-NiCr coating involves a change from a loosely packed orthorhombic structure to a closely packed hexagonal structure which is accompanied by a volume contraction. This volume contraction could induce significant residual stresses in the coating. It is believed that the cohesive strength (particle-to-particle bonding) of the coating is higher than its adhesive strength (particle-to-substrate bonding). An increase in residual stresses in the coating can increase probability of rupturing the coating-substrate bonding. It is common knowledge that continuing to increase the coating thickness (i.e., increasing residual stresses) during spraying can eventually spall the coating from the substrate. The combination of increased

residual stresses in the coating, due to phase transformation, and the occurrence of interfacial oxidation leads to faster spallation for the Cr_3C_2-NiCr coatings.

Figure 5 summarizes the spallation data generated so far for chromium carbide coatings on Alloy 800 (or Alloy 800H) substrate applied by various processes and vendors. The physical properties and bond strength of these coatings are tabulated in Table 3. Photomicrographs showing the typical optical microstructure of each coating are shown in Fig. 6.

The structures of the sprayed coatings are not very well understood. It is difficult at this point to make correlation between coating process, coating structure and properties, and spallation resistance. Nevertheless, the following observations can be summarized to qualitatively illustrate the relative spallation resistance of various sprayed coatings:

1. The Cr_3C_2-NiCr coating spalled faster than the $Cr_{23}C_6$-NiCr coating as discussed previously. This is not only true for plasma-sprayed coatings, but also for Detonation-gun applied coatings.

2. The application of a bond coat of NiCr layer between the coating and the substrate significantly increases the spallation resistance of the plasma-sprayed coatings. This is probably due to increased bonding between the coating and the substrate by the NiCr layer.

3. Detonation-gun applied coatings are much superior to plasma-sprayed coatings. The coatings applied by some high energy plasma processes are also superior to plasma-sprayed coatings, while those applied by others are not.

3.3. EFFECTS OF PLASMA SPRAYED $Cr_{23}C_6$-NiCr COATING ON LOW CYCLE FATIGUE AND CREEP RUPTURE PROPERTIES OF THE SUBSTRATE ALLOY 800H.

The principal areas to be protected from wear damage in steam generators are at points where the steam tubing contacts the support plates which separate neighboring tubes in the tube bundle. Relative movement between the tube and support plate can occur as a result of flow induced vibration, and thermal expansion and contraction of both tube and plate during thermal transients. To protect these tubes from wear damage, direct coating of the steam tubing with a chromium carbide based coating has been considered. The steam generator tubing is a primary coolant pressure boundary designed to meet the rules of the ASME Boiler and Pressure Vessel Code Section III Class 1 and Code Case 1592-10. Thus, it is necessary to obtain an accurate assessment of the effects of the coating on important design properties, such as creep rupture and low cycle fatigue properties. In this section the effects of the plasma-sprayed $Cr_{23}C_6$-NiCr coating* on the creep rupture and low cycle fatigue properties of a steam generator tubing material, Alloy 800H, are discussed.

3.3.1. Creep Rupture Properties

The creep rupture properties of uncoated, as-grit blasted, and coated specimens are summarized in Table 4. The stress rupture properties are summarized in Fig. 7(a). Stresses used for 1100°F (593°C) testing resulted in more than 4% strain during initial loading. As a result, the coating generally spalled off from the substrate. However, the stresses used for

*Linde's plasma-sprayed coatings.

1400°F (760°C) testing produced less than 1% strain during initial loading. Although the coatings contained numerous cracks, they normally stayed on the substrate even after rupture with elongation up to more than 70%. The coated specimens exhibited more surface cracks and fewer internal cracks compared to the uncoated specimens. Overall, the results revealed no significant effects on creep rupture properties due to the presence of the coating.

3.3.2. Low Cycle Fatigue Properties

The results of low cycle fatigue tests conducted in a continuous cyclic mode at 1100°F (593°C) are summarized in a plot of the total strain range versus the cycle to failure (N_5) as shown in Fig. 7(b). The fatigue life expressed as N_5 is the number of cycles at which the tensile load has decreased 5% from the maximum or cyclically stable value. The surface finish of the specimens varied from 16 μin. (0.04 μm) AA for uncoated specimens to approximately 200 μin. (5 μm) AA for both as-grit blasted and as-coated specimens. The fatigue life of the as-grit blasted specimen was comparable to that of the uncoated specimen. However, the fatigue life at 1.0% strain range was reduced from 2000 cycles for the uncoated specimen to 1290 cycles for the as-coated specimen. At 0.6% strain range the fatigue life was reduced from 10,550 cycles to 3801 cycles (nearly a factor of 3). Furthermore polishing the coating to improve the surface finish to approximately 22 μin. (0.5 μm) AA (comparable to that of the uncoated specimen) did not appear to significantly improve the fatigue life. Figure 7(b) shows that the deleterious effect of the coating on fatigue properties increases with decreasing total strain range.

The uncoated and grit blasted specimens had a macroscopic fracture appearance distinctly different from that of the coated specimen. The former exhibited a jagged fracture surface while the latter a flat fracture surface. The microscopic fracture appearance, as revealed by scanning electron microscopy, however, appeared to be similar. Both exhibited similar fatigue striations. For both strain ranges, no spallation or delamination of the coating was observed. For the specimens tested in both strain ranges, the coating near the fracture normally exhibited several microcracks which propagated through the coating and into the substrate. The plasma-sprayed coating generally contained some grit inclusions* at the coating-substrate interface. No definitive evidence was observed which suggested that microcracks were initiated from these grit inclusions.

---

*Some alumina grits were often entrapped on the substrate surface during grit blasting which is a process used to roughen the substrate surface prior to plasma spraying the coating.

4. SUMMARY AND CONCLUSIONS

1. The tribology of the sprayed chromium carbide-nichrome coatings is strongly dependent upon, among other factors, the sliding velocity. Decreasing the sliding velocity tends to increase the friction coefficient and to produce the chattering (stick-slip) phenomenon.

2. Sprayed chromium carbide-nichrome coatings could suffer spallation when exposed to a simulated HTGR helium environment at elevated temperatures. Spallation of the coating is believed to be primarily due to the formation of nearly continuous interfacial oxides which weaken the coating-substrate bonding. The instability of the carbide phase (e.g., a structural change from Cr_3C_2 to Cr_7C_3) in the coating can further promote spallation. Accordingly, Cr_3C_2-NiCr coatings spalled faster than $Cr_{23}C_6$-NiCr coatings. This is not only true for plasma-sprayed coatings, but also for Detonation-gun applied coatings. The application of a bond coat of NiCr layer between the coating and the substrate significantly increases the spallation resistance of the plasma-sprayed coatings. Detonation-gun applied coatings are much superior to plasma-sprayed coatings. The coatings applied by some high energy plasma processes are also superior to plasma-sprayed coatings, while those applied by others are not.

3. The presence of the plasma-sprayed $Cr_{23}C_6$-NiCr coating did not significantly affect the creep rupture properties of substrate Alloy 800H. The low cycle fatigue life was reduced by the presence of the plasma-sprayed $Cr_{23}C_6$-NiCr coating when tested at 1100°F (593°C) with 1.0% and 0.6% total strain ranges. The reduction in fatigue life increases with decreasing total strain range.

ACKNOWLEDGEMENT

The author greatly acknowledges the assistance given by Mrs. L. Holm and Mr. R. Frazee in conducting helium compatibility tests and friction and wear tests, Mr. E. Neff and Dr. C. Young in low cycle fatigue testing, Mr. J. Yaker, Mr. R. Pitylak and Professor W.C. Leslie of University of Michigan where creep rupture tests were conducted, Mr. J. Knipping and R. Spears in optical metallography, Mr. D. Wall in scanning electron microscopy, and Dr. P. Gantzel in X-ray diffraction analysis. The author is also grateful to Mrs. L. Holm and Dr. C. Li for assistance in preparing the manuscript, Mr. D.I. Roberts and Dr. J.E. Sheehan for reviewing the manuscript and valuable discussion, and Dr. J.F. Watson for continued support during the course of this investigation.

The work was supported in part by the Department of Energy under Contract EY-76-C-03-0167, Project Agreement No. 50.

REFERENCES

1. Burnette, R.D., W.E. Bell, L.R. Zumwalt, and C.A. Perry, "Evaluation of Carbon Transport Phenomena in HTGR Systems," GA-8624, General Atomic Company, San Diego, CA, October 1968.

2. Grebetz, J.C., "The Unlubricated Friction and Wear Behavior of Structural Materials in Helium at 800°C," GA-8697, General Atomic Company, San Diego, CA, July 1968.

3. Mazandarany, F.N., "Effects of Elevated Temperature Exposure to a Simulated HTGR Primary Coolant Environment on Several Unstressed Austenitic Alloys," GA-A13462, General Atomic Company, San Diego, CA, August 1975.

4. Slot, T., R.H. Stenty, J.T. Berling, "Controlled-Strain Testing Procedures," Manual on Low Cycle Fatigue Testing, ASTM S.T.P. 465, ASTM, Philadelphia, Pa., 1969.

5. Smith, G.V., The Properties of Metals at Elevated Temperatures, McGraw-Hill, New York, p. 179, 1950.

6. Taylor, T.A., "Phase Stability of Chrome-Carbide NiCr Coatings in Low-Oxygen Environment," J. Vac. Sci. Technol., Vol. 12, No. 4, July-August 1975.

7. Mazandarany, F.N., and R.D. Pehlke, Met. Trans., 4, p. 2067, 1973.

TABLE 1
CHEMICAL COMPOSITIONS OF THE SUBSTRATE MATERIALS UNDER INVESTIGATION

Material	Heat Treatment	Chemical Composition (wt %)[a]													
		C	Fe	Ni	Cr	Co	Mo	Al	Ti	Mn	Si	S	P	Cu	Other
Hastelloy X[b]	Solution-Annealed	0.06	18.97	Bal.	22.31	2.11	8.55	--	--	0.61	0.25	0.005	0.022	--	W-0.62 B-<0.002
Alloy 800[c]	Solution-Annealed	0.03	44.38	32.81	20.14	--	--	0.41	0.49	0.85	0.34	0.007	--	0.52	
Alloy 800H[d]	Solution-Annealed	0.08	45.21	31.97	20.63	--	--	0.32	0.26	0.93	0.41	0.007	--	0.16	

(a) Vendor's analysis.

(b) Substrate material for friction and wear test specimens. The specimens are 0.25 in. diameter x 0.13 in. long buttons and 0.375 in. thick x 0.5 in. wide x 1.0 in. long plate specimens. The coating is applied on flat face of the button, and on both top and bottom sides of the plate specimen.

(c) Substrate material for helium compatibility test specimens (flat disk specimens). The specimen is 0.1 in. thick x 1 in. diameter. The coating is applied on one side of the test specimen.

(d) Substrate material for helium compatibility test specimens (0.5 in. diameter x 3 in. long round specimens), creep-rupture specimens (0.25 in. diameter x 1 in. gage length), and low cycle fatigue specimens (0.25 in. diameter hour-glass specimen). The coating is applied on the midsection (2 in. long) of helium compatibility test specimens, and on the reduced section of both creep and low cycle fatigue specimens. The grain size of this heat of material was ASTM No. 4.

TABLE 2
RESULTS OF X-RAY DIFFRACTION ANALYSIS OF THE PHASES PRESENT IN LINDE'S PLASMA SPRAYED Cr_3C_2-NiCr AND $Cr_{23}C_6$-NiCr COATINGS

Coating	Coating Condition	Phases Present						
		$Cr_{0.62}C_{0.35}N_{0.03}$	Cr_3C_2	Cr_7C_3	$Cr_{23}C_6$	NiCr	Cr_2O_3	$FeCr_2O_4$ Type Spinels
Cr_3C_2-NiCr	As-coated[a]	Major	Minor	Minor	--	Major	--	--
	1600°F/1 hr[a]	--	Major	Minor	--	Major	--	--
	1600°F/ 520 hr[b]	--	Major	Major	--	Major	--	--
$Cr_{23}C_6$-NiCr	As-coated[a]	--	--	--	Weak Pattern	Weak Pattern	--	--
	1600°F/1 hr[a]	--	--	Minor	Major	Major	Minor	--
	1600°F/ 2700 hr[b]	--	--	--	Major	Major	--	Minor

(a) Coating mechanically removed for analysis.

(b) Coating spalled after exposure.

TABLE 3
PHYSICAL PROPERTIES AND BOND STRENGTH OF VARIOUS CHROMIUM CARBIDE COATINGS (ALLOY 800 SUBSTRATE)

Type of Coating	Vendor	Apparent[(a)] Density (g/cc)	Bond[(b)] Strength psi(MPa)	Microhardness[(c)] (DPH)
Plasma Cr_3C_2-NiCr	Linde	5.93	9,740(67.16) 9,960(68.67)	698
Plasma $Cr_{23}C_6$-NiCr	Linde	(d)	8,910(61.43) 10,420(71.85)	792
Plasma $Cr_{23}C_6$-NiCr/NiCr[(e)]	Linde	6.02	9,190(63.37) 9,680(66.74)	654
D-gun Cr_3C_2-NiCr	Linde	6.50	10,360(71.43) 10,750(74.12)	859
D-gun $Cr_{23}C_6$-NiCr	Linde	6.39	9,350(64.47) 9,700(66.88)	681
High Energy Plasma Cr_3C_2-NiCr	Pratt & Whitney	(d)	10,260(70.74) 10,350(71.36)	665
High Energy Plasma $Cr_{23}C_6$-NiCr	Plasmadyne	7.0	8,300(57.23) 11,900(82.05)	523
High Energy Plasma Graded $Cr_{23}C_6$-NiCr[(f)]	Plasmadyne	6.77	12,030(82.95) 12,600(86.88)	672

(a) Measured at 1 atm.
(b) Measured by Vendor.
(c) Average of 10 measurements using 300g load.
(d) Samples not enough for measurements.
(e) Duplex coating with a bond coat of NiCr layer (0.002 in. thick) between the $Cr_{23}C_6$-NiCr coating and the substrate.
(f) Composition of carbide varies from 0% at the interface to 100% at the coating surface, while NiCr varies from 100% to 0%.

TABLE 4

SUMMARY OF CREEP RUPTURE PROPERTIES OF UNCOATED, AS-GRIT BLASTED AND COATED* ALLOY 800H SPECIMENS.

Specimen Condition	Testing Temperature °F (°C)	Stress Ksi(MPa)	Strain due to initial loading (%)	Secondary Creep Rate (%/hr)	Time to Tertiary Creep (hr)	Time to Rupture (hr)	Elongation (%)	Reduction in Area (%)
uncoated	1100(593)	50(344.7)	15	1.38×10^{-1}	55	71.5	26.7	24.9
uncoated	1100(593)	45(310.3)	11.7	1.54×10^{-2}	91	137.4	26.6	31.2
uncoated	1100(593)	35(241.3)	4.4	4.0×10^{-3}	237.5	610	24.0	25.1
as-grit blasted	1100(593)	45(310.3)	10.8	1.25×10^{-2}	80	137.7	23.2	22.9
as-coated	1100(593)	50(344.7)	14.8	5.0×10^{-2}	43	58.1	21.4	20.6
as-coated	1100(593)	45(310.3)	11.05	1.0×10^{-2}	97	152.6	17.1	22.2
as-coated	1100(593)	35(241.3)	5.5	2.2×10^{-3}	280	782.9	17.3	17.6
uncoated	1400(760)	16(110.3)	0.41	5.5×10^{-1}	29	46.9	57.8	53.7
uncoated	1400(760)	12(82.7)	0.07	1.3×10^{-1}	123	200.9	74.5	57.6
uncoated	1400(760)	9(62)	0.14	1.07×10^{-2}	675	1622.6	36.2	25.2
as-grit blasted	1400(760)	12(82.7)	0.05	1.43×10^{-1}	115	198.8	63.2	43.2
as-coated	1400(760)	16(110.3)	0.15	8.0×10^{-1}	13.5	32.4	58.6	52.0
as-coated	1400(760)	12(82.7)	0.15	1.2×10^{-1}	90	222.3	43.1	34.0
as-coated	1400(760)	9(62)	0.25	1.56×10^{-2}	500	1410	40.8	25.6

*Linde's plasma-sprayed $Cr_{23}C_6$-NiCr coating.

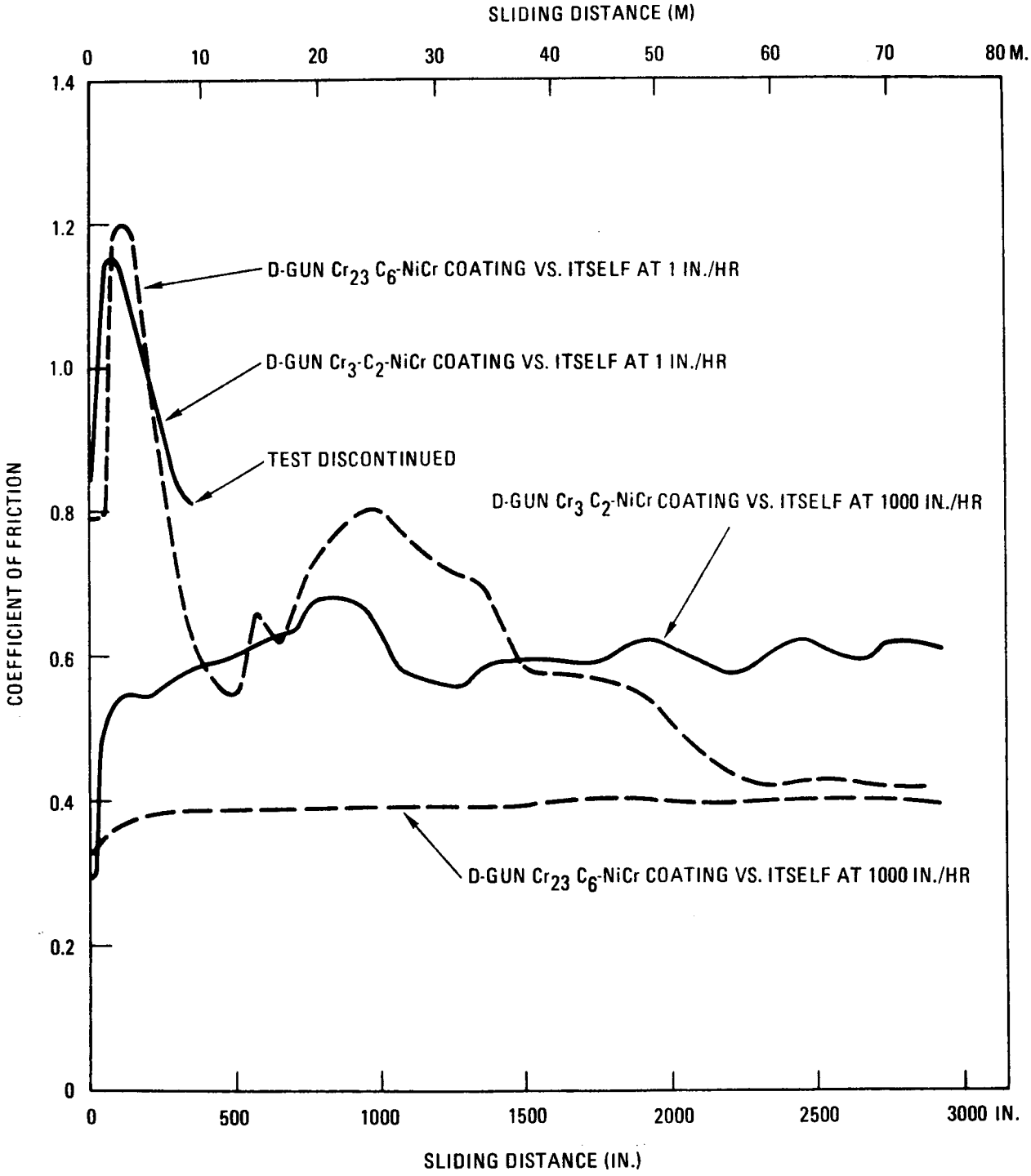

Fig. 1. Friction coefficient (maximum value) as a function of sliding distance for the chromium carbide-nichrome coating rubbing against itself at 1500°F (816°C) and 500 psi (3.45 MPa) with two different sliding velocities. The surface finish of the coated specimens was about 100 μin AA.

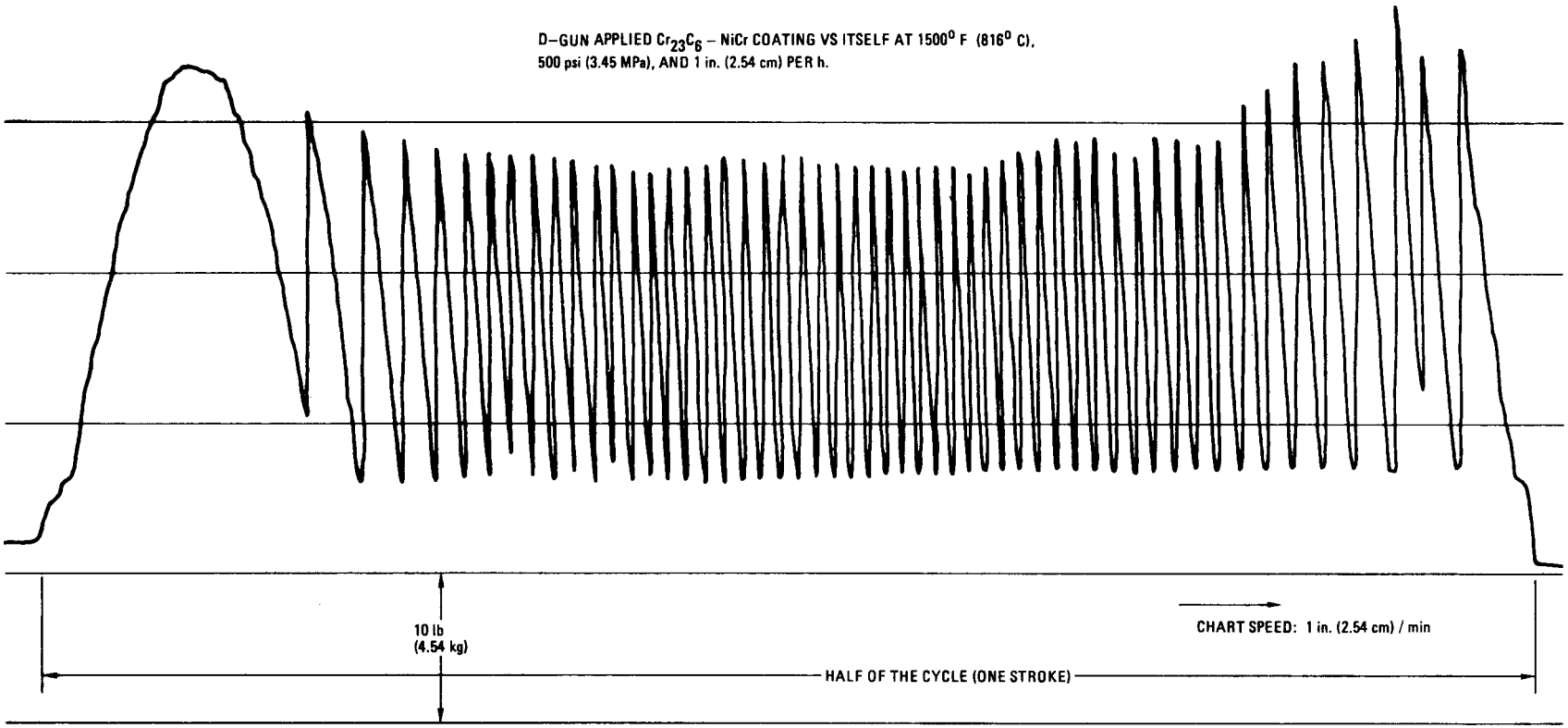

Fig. 2. Typical frictional force trace showing the observed chattering during sliding half of the cycle or one stroke (0.25 in. (0.635 cm)).

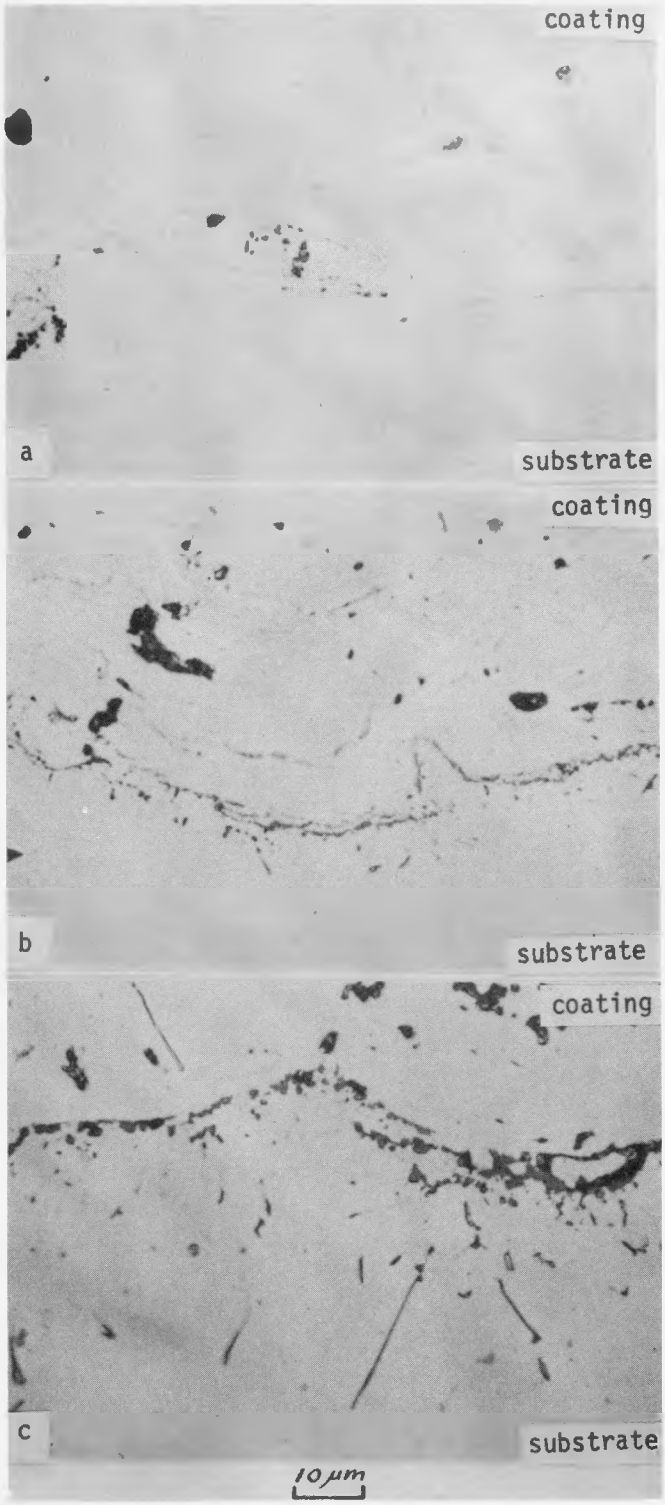

Fig. 3. Typical optical microstructure of plasma $Cr_{23}C_6$-NiCr coated Alloy 800H after exposure to a simulated HTGR He environment at (a) 1200°F/1076 hr, (b) 1400°F/1006 hr and (c) 1600°F/1076 hr; unetched.

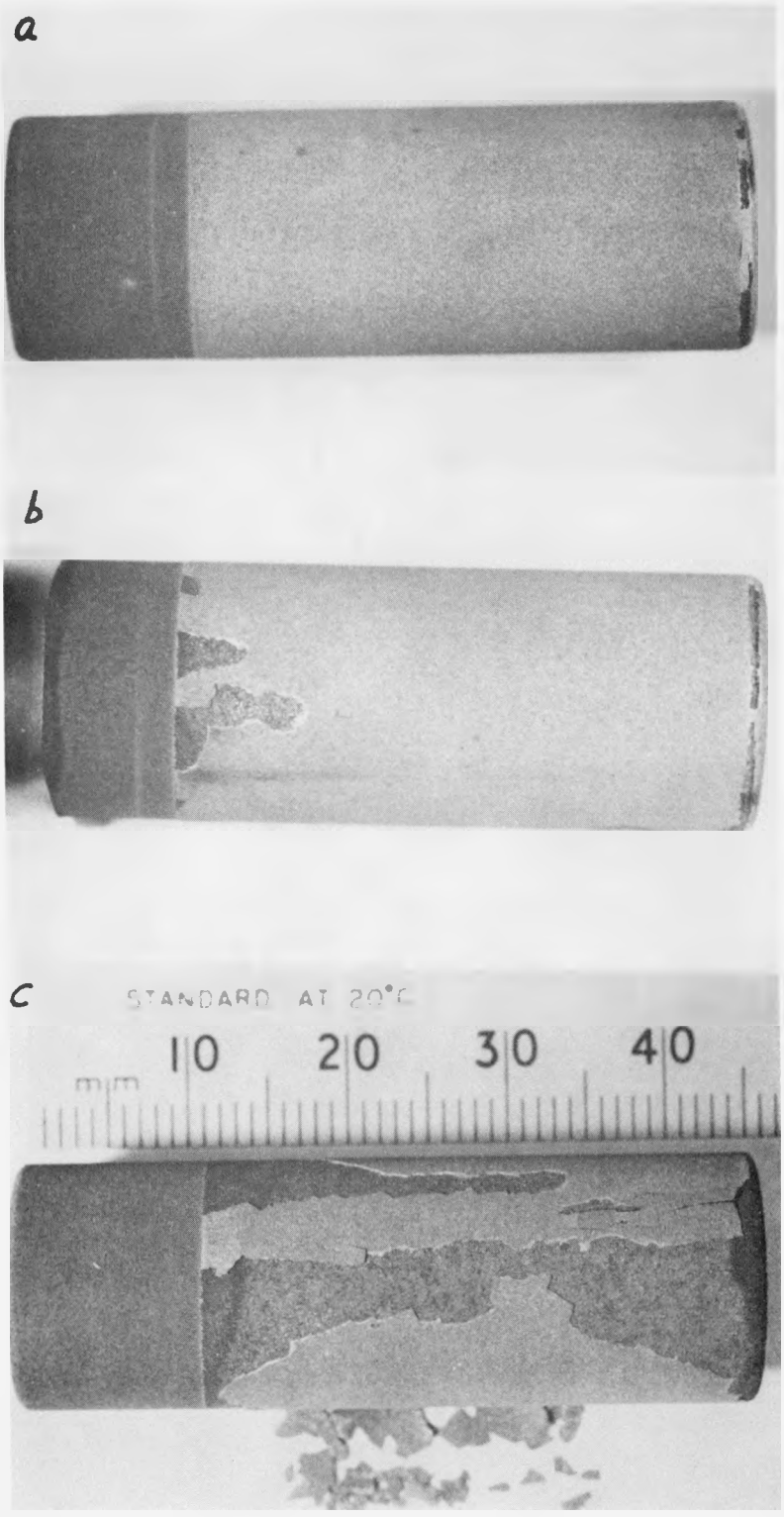

Fig. 4. Plasma $Cr_{23}C_6$-NiCr coated Alloy 800H specimens after exposure to a simulated HTGR He environment at 1600°F (871°C) for (a) 1578 hr, (b) 1914 hr, and (c) 2610 hr.

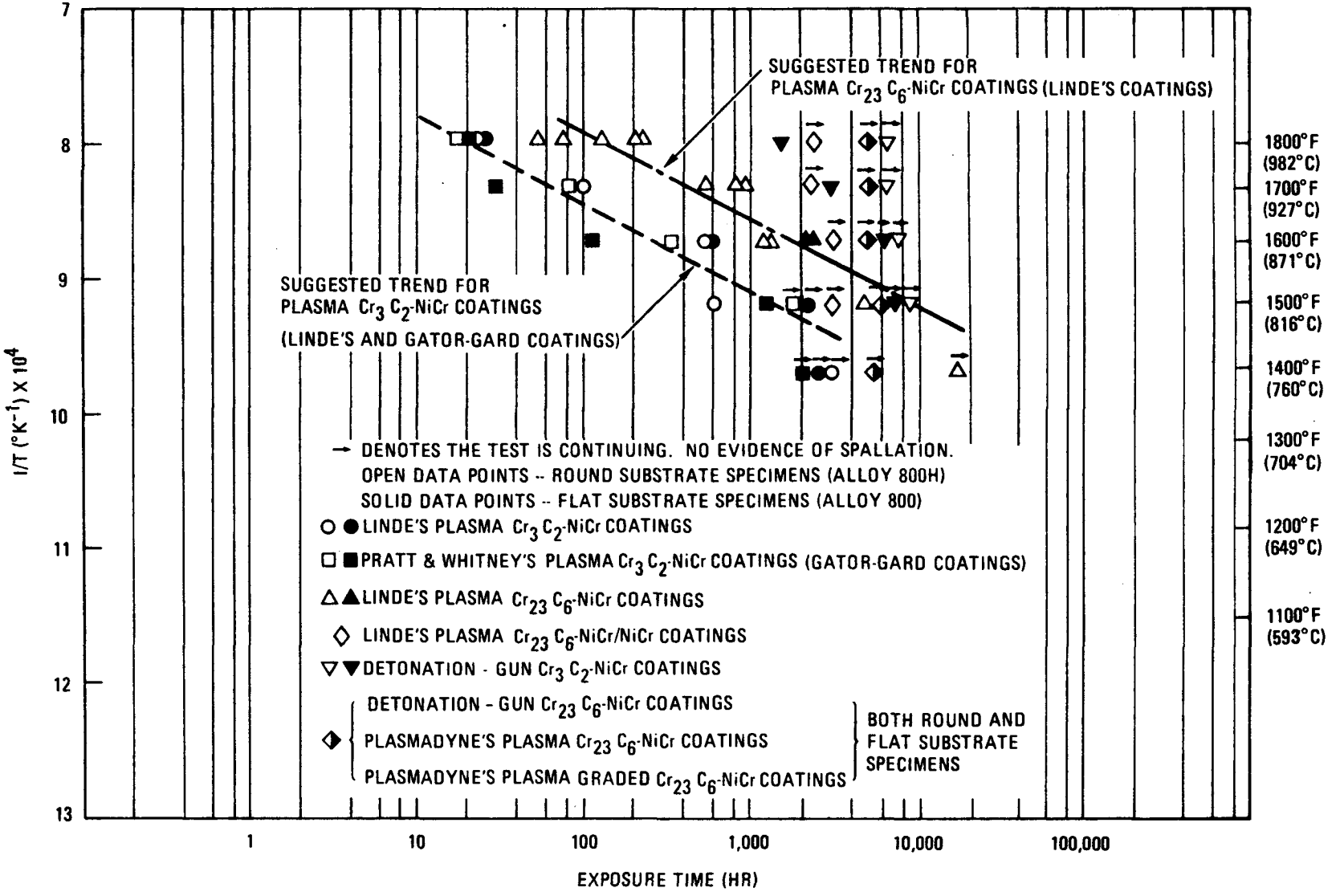

Fig. 5. Spallation data generated so far for various chromium carbide-nichrome coatings are presented in a plot of 1/T vs. the exposure time when the spallation of coating was observed.

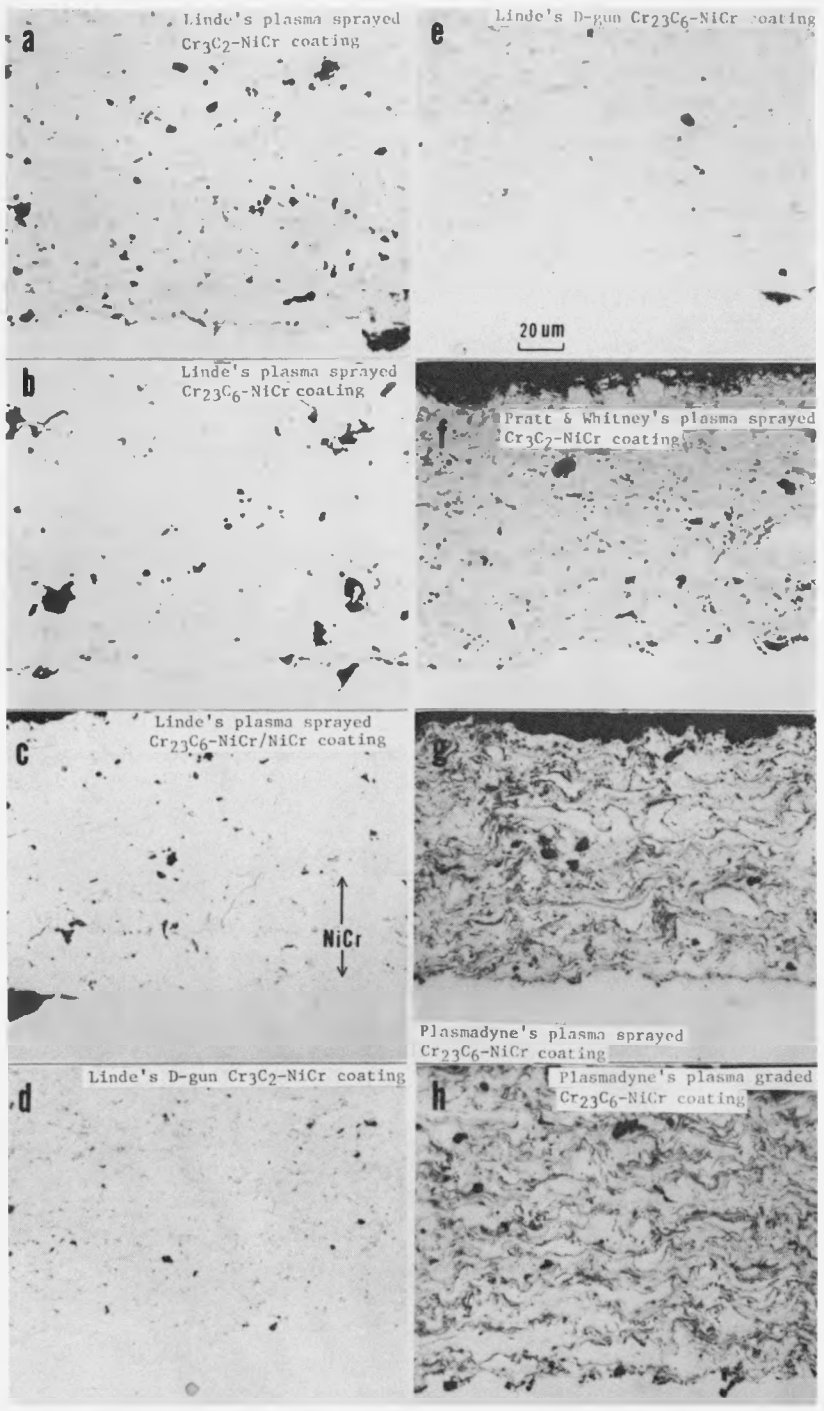

Fig. 6. Typical optical microstructure of (a) Linde's plasma sprayed Cr_3C_2-NiCr coating, (b) Linde's plasma sprayed $Cr_{23}C_6$-NiCr coating, (c) Linde's plasma sprayed $Cr_{23}C_6$-NiCr/NiCr coating, (d) Linde's D-gun Cr_3C_2-NiCr coating, (e) Linde's D-gun $Cr_{23}C_6$-NiCr coating, (f) Pratt & Whitney's plasma sprayed Cr_3C_2-NiCr coating, (g) Plasmadyne's plasma sprayed $Cr_{23}C_6$-NiCr coating, and (h) Plasmadyne's plasma graded $Cr_{23}C_6$-NiCr coating. Unetched.

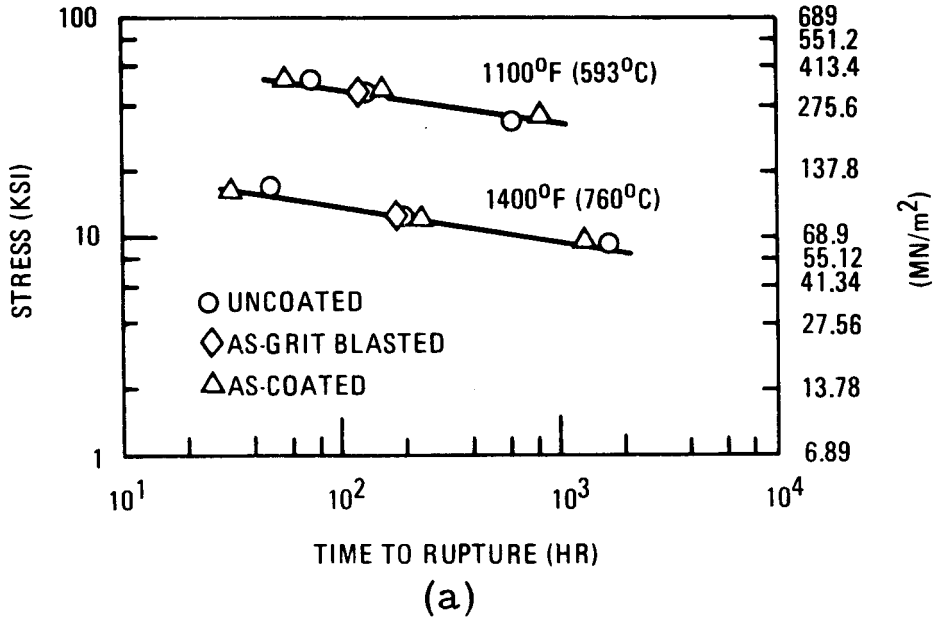

(a)

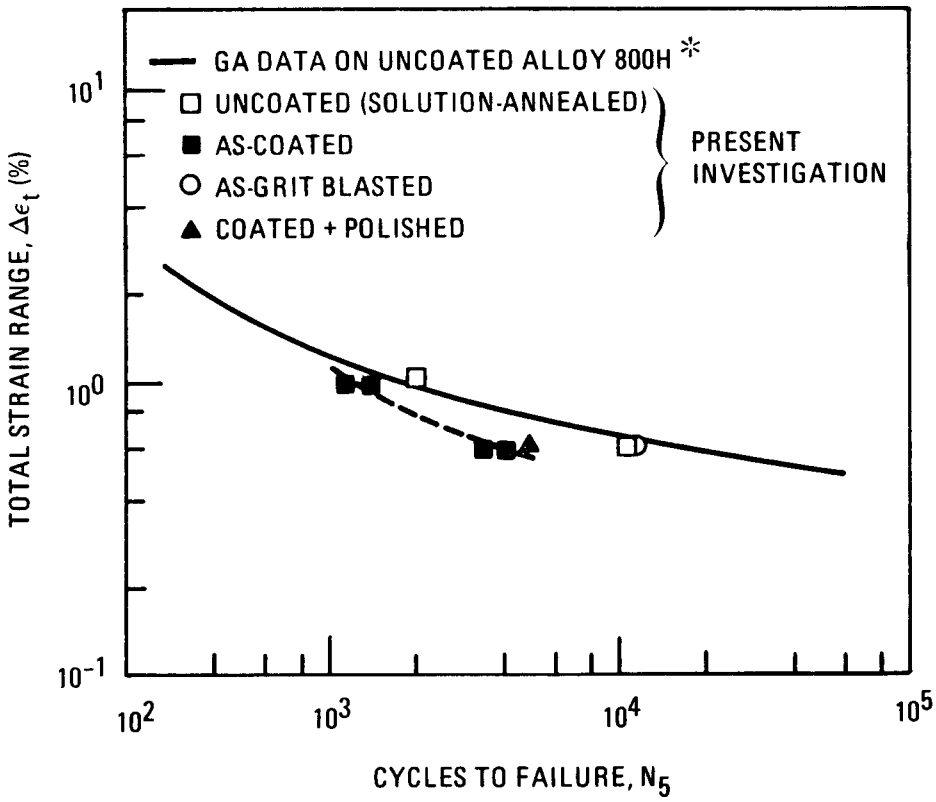

(b)

Fig. 7. Stress-rupture properties (a) and low cycle fatigue properties at 1100°F (593°C) (b) of uncoated, as-grit blasted, and coated** Alloy 800H specimens. *Material of different heat. **Linde's plasma-sprayed $Cr_{23}C_6$-NiCr coating.